mater.scichina.com link.springer.com

Sci China Mater 2025, 68(7): 2433–2441
https://doi.org/10.1007/s40843-025-3354-3

From lunar glass to advanced metallic glass: dense nanocrystallization catalyzed by implanted ions

Xiao Chen[1,2], Benshun Ma[1,2], Lijian Song[1*], Yan Zhang[1,2*], Yongjiang Huang[3*], Jianfei Sun[3], Wei Xu[1], Ao Li[1], Jianing Wang[1,2], Hanboce Yin[1], Bowen Zang[1], Meng Gao[1], Shaofan Zhao[4], Wei Yao[4], Zhigang Zou[4,5], Mengfei Yang[4], Weihua Wang[2,4,6,7], Haiyang Bai[2,4,6], Juntao Huo[1,2*] and Jun-Qiang Wang[1,2*]

ABSTRACT Nanocrystallization of glasses is a critical pathway for designing advanced materials with superior properties. In this study, we investigated the crystallization behavior of lunar glasses retrieved by the Chang'E-5 mission. It was observed that solar wind irradiation induces abundant Fe nano-clusters with a size of about 2 nm within a layer of about 4 μm close to the surface. Upon heating, these defects act as nucleation sites, facilitating the precipitation of homogeneous and dense Fe nanocrystals. In contrast, the unirradiated interior of the lunar glass crystallizes into coarse Fe crystals. Inspired by these findings, advanced magnetic nanocrystalline alloys are designed based on $Fe_{86}B_{14}$ metallic glass by H^+ ion irradiation. After H^+ ion irradiation and nanocrystallization, the size of nanocrystals close to the surface is about 5–8 nm, which is much smaller than the nanocrystals in the deep interior (15–20 nm). The permeability at 10 kHz increases by about 10.2%. These results not only give insights into the thermal stability of lunar glasses, but also present a novel strategy for designing advanced soft magnetic materials with enhanced performance.

Keywords: lunar glasses, solar wind, ion irradiation, Fe-based metallic glass, *in situ* TEM, nanocrystallization

INTRODUCTION

Lunar glasses are widely distributed on the Moon, constituting up to 20–30 vol% of the lunar surface regolith [1,2]. These glasses can be primarily categorized into two types: volcanic glasses and impact glasses [3–5]. Volcanic glasses form from the fast cooling of the melt of volcanic eruptions or melted ejecta triggered by hypervelocity impacts [3,6,7], which provide critical information regarding the Moon's interior evolution [6,8,9]. These glasses offer valuable insights into the cooling and solidification processes of the early lunar mantle [8,10]. Impact glasses, on the other hand, are formed by the melting and rapid quenching of diverse lunar surface materials during impact events [3,6,11]. They are valuable for investigating the composition of various lunar regions and for confirming the timing of impact events [12,13]. Impact glasses can be generated through both massive basin-forming impacts and smaller meteorite impacts [1,14,15]. There are usually thin amorphous rims on the surface of lunar particles [16,17], which could be formed by the irradiation of cosmic and solar wind ions or by accreting silicate vapor [18–22]. However, the thicknesses of these amorphous rims are typically less than 2 μm thick, which is much smaller than volcanic and impact glasses on the Moon. Lunar glasses not only provide geological insights into the origin and evolution of the Moon, but also hold significant potential for *in situ* resource utilization (ISRU) in future lunar missions [23]. Their long-term stability [24] and abundance [25] make them valuable for both scientific investigation and practical applications in lunar exploration.

The absence of an atmosphere on the Moon exposes lunar glasses to continuous solar wind irradiation, which significantly affects their structure and properties over time. For instance, the irradiated rims of lunar glasses play a crucial role in retaining solar-derived elements such as helium (He) and hydrogen (H) [26]. The retained 3He is considered a potential strategic energy resource [27], while hydrogen may interact with lunar minerals to produce water [28–34]. Solar wind irradiation also impacts the thermal stability and crystallization behavior of lunar glasses. Understanding the crystallization mechanisms of these glasses is essential for the selection and design of advanced materials required for future lunar and interplanetary exploration. Additionally, the study of the crystallization behavior of lunar glasses, which possess complex chemical compositions—including major elements such as O, Si, Fe, Mg, Al, Ca, and Ti [4,35], as well as minor elements such as Na, K, and S—can provide insights into the thermal stability of lunar glasses [4]. These

[1] CAS Key Laboratory of Magnetic Materials and Devices, and Zhejiang Province Key Laboratory of Magnetic Materials and Application Technology, Ningbo Institute of Materials Technology and Engineering, Chinese Academy of Sciences, Ningbo 315201, China
[2] Center of Materials Science and Optoelectronics Engineering, University of Chinese Academy of Sciences, Beijing 100049, China
[3] School of Materials Science and Engineering, Harbin Institute of Technology, Harbin 150001, China
[4] Qian Xuesen Laboratory of Space Technology, China Academy of Space Technology (CAST), Beijing 100049, China
[5] College of Engineering and Applied Science, Nanjing University, Nanjing 210093, China
[6] Institute of Physics, Chinese Academy of Sciences, Beijing 100049, China
[7] Songshan Lake Materials Laboratory, Dongguan 523830, China
[*] Corresponding author (email: songlj@nimte.ac.cn; yzhang@nimte.ac.cn; yjhuang@hit.edu.cn; huojuntao@nimte.ac.cn; jqwang@nimte.ac.cn)

studies may inform the design and development of advanced soft magnetic nanocrystalline materials for various technological applications.

In this study, several typical lunar glass particles of varying sizes were selected from the lunar regolith samples returned by the Chang'E-5 mission [25,36–39]. Due to the small size of these particles, their microstructure and thermodynamic properties were analyzed in detail using microscopic techniques, including scanning electron microscopy (SEM), transmission electron microscopy (TEM), and Flash differential scanning calorimetry (FDSC). Additionally, the nanocrystallization process was directly observed through *in situ* heating TEM experiments. The results indicate that the nanocrystallization mechanism is significantly influenced by solar wind irradiation. Since over 90% of the solar wind consists of hydrogen ions [40], hydrogen ion irradiation was applied to Fe-based metallic glasses to simulate the effects of solar wind irradiation. The structure of Fe-based metallic glass after hydrogen ion irradiation closely resembles that of lunar glasses. Similarly, its crystallization behavior at high temperatures shows strong similarities to that of lunar glasses. This confirms that hydrogen ion irradiation, analogous to solar wind irradiation, is an effective method for achieving a uniform and ultrafine nanocrystal distribution. These findings not only elucidate the thermodynamic properties and crystallization behavior of lunar regolith glasses but also reveal a novel approach inspired by lunar regolith for controlling nanocrystalline soft magnetic materials. This method has significant implications for the design and performance optimization of advanced materials.

MATERIALS AND METHODS

Lunar glasses sorting

The Chang'E-5 sample studied in this work was scooped from the lunar regolith surface (sample CE5C400) [41–43]. The lunar samples were stored in a glove box (by Mikrouna Inc.) under high-purity argon gas before and after being explored. On account of the typical spherical shape of lunar glasses, the lunar glasses samples were easy to pick out under optical microscope (NM910, by Ningbo Yongxing Inc.) in the glove box. The sizes of the sorted lunar glasses samples were about 20–100 μm.

FeB sample preparation and irradiation treatment

Ingot with a nominal composition of $Fe_{86}B_{14}$ (at%) was prepared through the arc melting of high-purity constituent elements in a Ti-gettered high purity argon atmosphere. $Fe_{86}B_{14}$ ribbons with a thickness of 10–11 μm and a width of 10–12 mm were prepared in an argon atmosphere by a single roller melt spinner using a copper wheel with a circumferential speed of 50 m s^{-1}. All the irradiation treatment of FeB sample was performed at Harbin Institute of Technology. The samples were irradiated in a high vacuum chamber of 6×10^{-4} Pa by H^+ ions with fluences of ~1×10^{17} ions cm^{-2} and an energy of 60 keV. Considering that the H^+ fluence of solar wind is 4.1×10^8 ions cm^{-2} s^{-1} [44]. The equivalent exposure age of irradiated FeB metallic glass is 2.43×10^8 s, which is equal to 7.7 years. Since the energy of H^+ irradiation on FeB metallic glass is 60 keV, which is much higher than that of solar wind (0.3–3 keV). Thus, the equivalent exposure age of irradiated FeB metallic glass should be higher than 7.7 years. The $Fe_{86}B_{14}$ ribbons were annealed at 653 K for 5 s. The relative permeability in the frequency range from 1 kHz to 1 MHz of $Fe_{86}B_{14}$ ribbons was measured using an impedance analyzer (WK6500B by Wayne Kerr) at 1 A m^{-1} in the external field.

Microstructure characterization

The morphology of lunar glass samples and irradiated FeB samples was characterized by field emission scanning electron microscope (SEM, Verios G4 UC by ThermoFisher), with an acceleration voltage of 15.0 kV and a probe current of 3.2 nA. The elements existing in the lunar glasses sample were determined by energy-dispersive X-ray spectroscopy (EDS, X-Man series by Oxford). TEM samples were prepared by a SEM with focused ion beam (FIB, Helios G4 CX by ThermoFisher) operated under 30 kV high tension and 0.79 nA current for thinning and 2 kV high tension and 39 pA current for polishing. The *in situ* heating experiments were performed in TEM (Talos F200X by ThermoFisher) after loading the sample on a specially designed chip sensor (by ThermoFisher). The FIB-milled sample was immediately transferred into the TEM to prevent potential oxidation. The *in situ* TEM sample was initially heated to 373 K. Then the sample was heated to the desired temperatures at the rate of 1 K s^{-1}. At each temperature, the sample was kept for 10 min and the high-resolution TEM (HRTEM) images were acquired. After *in situ* TEM heating experiments, the samples were cooled to room temperature for EDS characterization.

FDSC measurements

FDSC experiments of lunar glass samples were performed with a heating rate of 10 K s^{-1} using an FDSC equipped with the UFH sensor (Flash DSC 2+ by Mettler Toledo). 10 K s^{-1} is the lowest allowable heating rate for FDSC, which is close to the heating rate of the *in situ* heating TEM experiment. The upper temperature limit of FDSC is 1273 K. FDSC was done with an Ar gas flow with a constant rate of 80 mL min^{-1}.

RESULTS AND DISCUSSION

Fig. 1 presents the SEM images of various lunar glass particles and the FDSC curves for two specific samples. Fig. 1a shows nanometer-scale spherical glass particles, which are widely distributed on the surfaces of different lunar particles. Fig. 1b–e depict spherical glasses with diameters in the micron scale, ranging from approximately 20 to 100 μm. These glasses are primarily composed of elements such as O, Si, Mg, Al, Ca, Ti, and Fe, with some variation in their elemental compositions. The detailed elemental compositions and EDS mappings of these micron-sized glasses are provided in Table S1 and Fig. S1. Based on the SEM and EDS analyses, lunar glasses are classified as silicate glasses, with trace amounts of other elements. The thermal properties of lunar glasses were characterized using FDSC, as shown in Fig. 1f. The glass transition temperature (T_g) and crystallization temperature (T_x) for lunar glass sample 1 are approximately 944 and 1260 K, respectively. For lunar glass sample 2, these temperatures are approximately 968 and 1251 K, respectively. These results provide critical data for understanding the thermal behavior of lunar glasses.

As mentioned above, solar wind, primarily composed of H^+ ions, interacts strongly with the lunar regolith, leading to structural alterations of lunar glasses. Fig. 2a illustrates that long-term solar wind irradiation forms a thin irradiation layer close to the surface of lunar glasses. Despite this, the overall structure of the lunar glasses remains amorphous. HRTEM

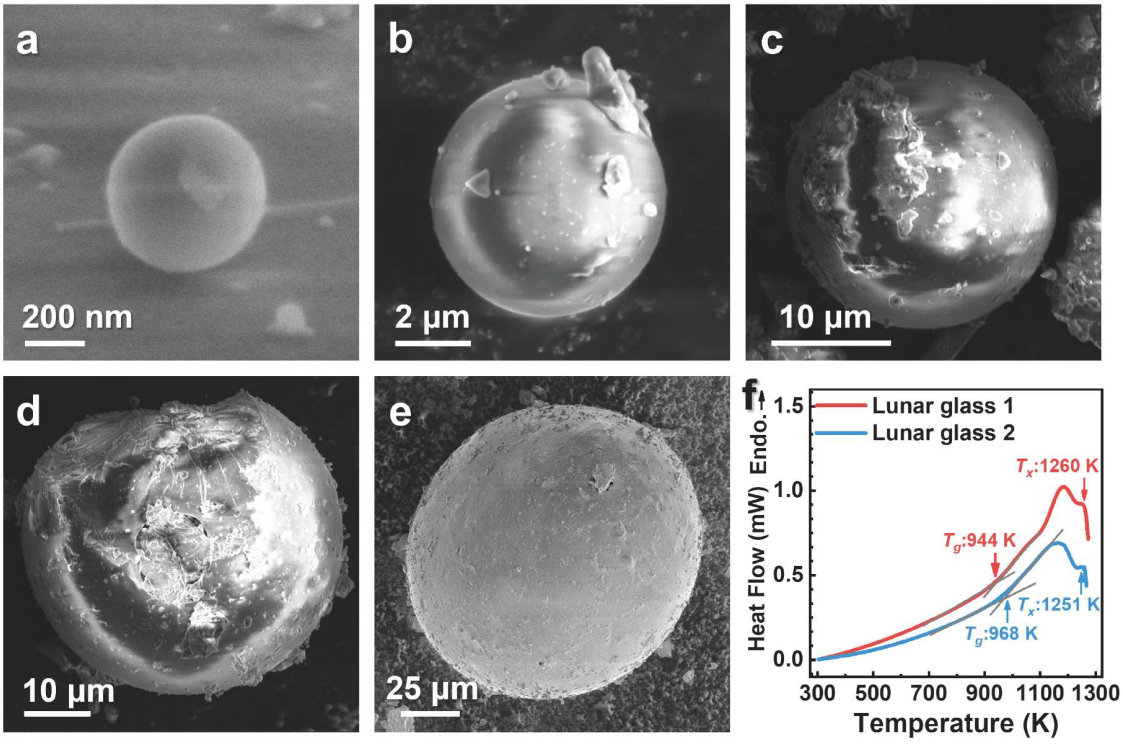

Figure 1 SEM images and Flash DSC curves of lunar glasses. (a) SEM image of nanometer spherical glasses distributed on the surface of different lunar minerals; (b–e) SEM images of spherical glasses with sizes of micron-scale; (f) Flash DSC curves of two lunar glass samples, the red and blue arrows represent the T_g and T_x temperatures of two lunar glass samples, respectively.

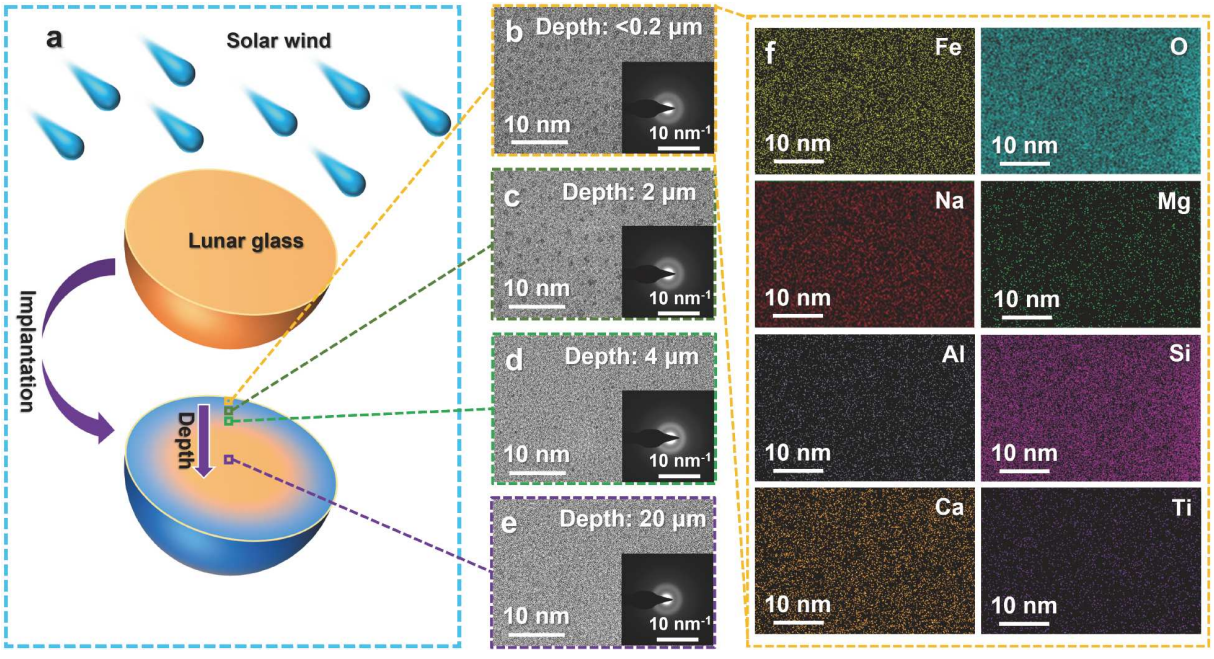

Figure 2 Microstructure of the cross-section of a lunar glass particle. (a) Schematic of solar wind implantation on lunar glasses, causing an irradiation layer close to the surface. (b–e) The HRTEM images of different depth of lunar glass; the insets show the SAED patterns: (b) Surficial layer (depth: <0.2 μm); (c) Depth: ~2 μm; (d) Depth: ~4 μm; (e) The interior part (depth: ~20 μm). (f) The HADDF image and EDS mapping (Fe, O, Na, Mg, Al, Si, Ca, Ti) close to the surface in the lunar glass.

images (Fig. 2b, c) reveal the presence of dark clusters approximately 2–3 nm in size, which distribute uniformly in the lunar glasses close to the surface. The selected area electron diffraction (SAED) patterns shown in the insets of Fig. 2b, c confirm this amorphous nature. As the depth increases, the density of these clusters gradually decreases. At a depth of

approximately 4 μm, the clusters almost vanish, suggesting that the effect of solar wind implantation weakens significantly. This is further supported by the observation of the central region of the lunar glass particle (depth ~20 μm, Fig. 2e), where no clusters are present. Therefore, the irradiation layer within the lunar glasses is confined to a depth of less than 4 μm. Although dark clusters are observed within the irradiation layer, EDS mapping (Fig. 2f) reveals no evidence of elemental aggregation in these regions. This suggests that the structural changes induced by solar wind irradiation do not result in significant elemental segregation.

The crystallization behavior of lunar glasses was investigated using *in situ* TEM during heating to examine the influence of solar wind irradiation. In the irradiation layer close to surface, heating to 473 K (Fig. 3a) did not induce any observable changes in structure or chemical composition, as confirmed by the corresponding SAED pattern (inset of Fig. 3a). At 873 K, the structure remained fully glassy, with only slight growth of clusters (Fig. 3b). Upon heating to 933 K, a nanocrystal with a diameter of approximately 5 nm was first observed (inset at the top right in Fig. 3c). Lattice fringes confirmed the presence of nanocrystals. However, due to the early stage of nanocrystallization, the number and size of the nanocrystals were insufficient to produce any noticeable changes in the SAED pattern (inset at the lower right of Fig. 3c). As the temperature increased to 953 K, significant growth of the clusters was observed, with diameters reaching around 5 nm (Fig. 3d). Concurrently, the number density of clusters exhibiting lattice fringes also increased, indicating that these clusters were likely the precursors of nanocrystals. When the temperature exceeded 973 K,

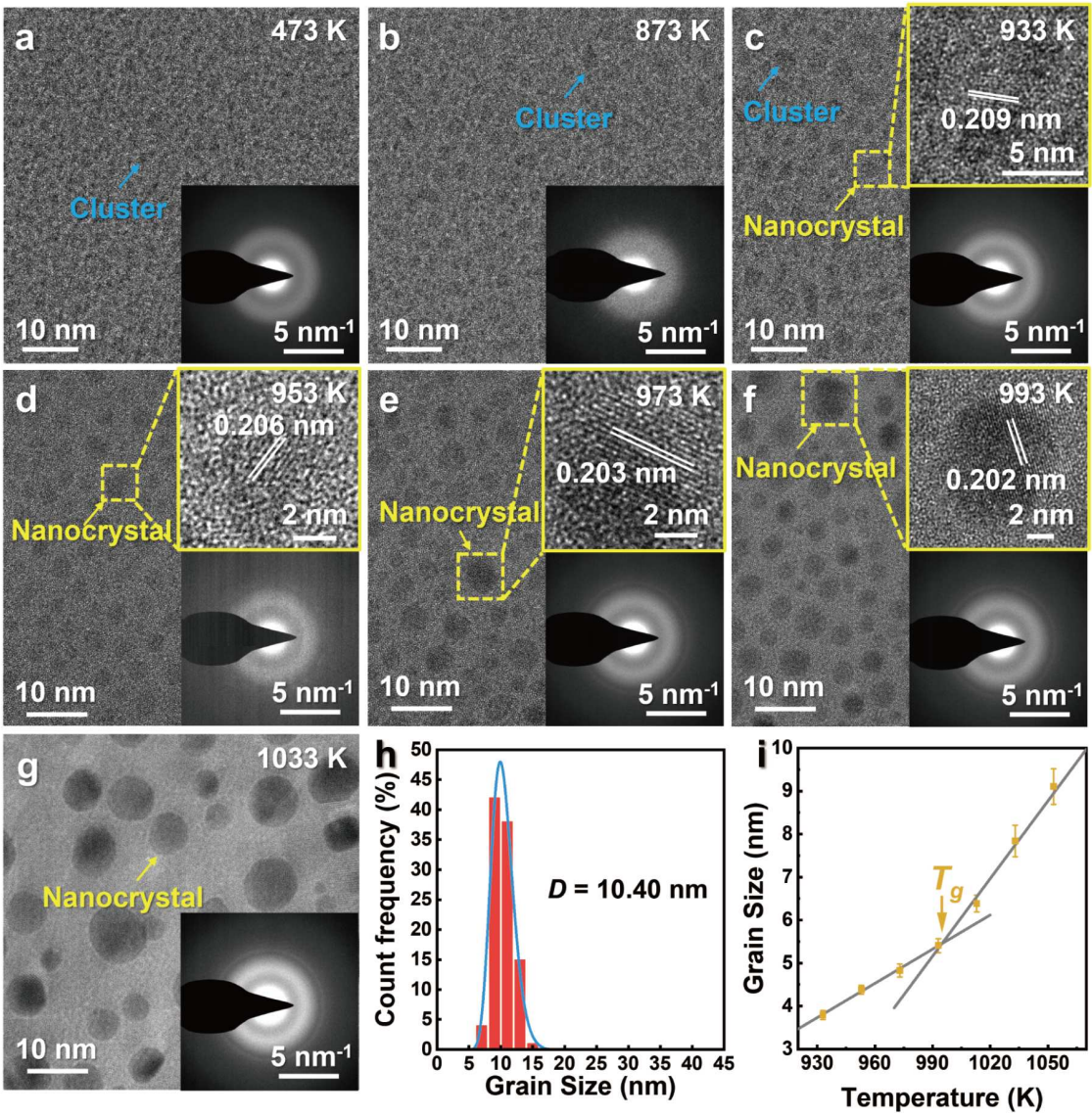

Figure 3 *In situ* HRTEM images and grain size distribution of the irradiation layer in the lunar glass at different stages of *in situ* heating TEM observation. The temperature and holding time at which the images were acquired are (a) 473 K, 10 min; (b) 873 K, 10 min; (c) 933 K, 10 min, the inset shows the lattice fringe is observed; (d) 953 K, 10 min; (e) 973 K, 10 min; (f) 993 K, 10 min; (g) 1033 K, 10 min. The blue arrows represent the clusters and the yellow arrows represent the nanocrystals. The insets show the zoomed-in HRTEM images of nanocrystals and corresponding SAED patterns. (h) The grain size distribution for the irradiation layer in the lunar glass after *in situ* TEM heating; (i) The trend of grain size variation with temperature in the irradiation layer. The intersection of the two grain growth stages represents the T_g temperature of the irradiation layer.

the clusters continued to grow, reaching approximately 8 nm in size, and the rate of transformation to the nanocrystalline phase accelerated (Fig. 3e, f). At 1033 K, the nanocrystals further grew and merged (Fig. 3g).

The size of the nanocrystals was statistically measured. As shown in Fig. 3h, i, the average grain size of the nanocrystals in the irradiation layer is 10.40 nm. These nanocrystals are uniformly distributed within the amorphous matrix. As the temperature increases, the grain size of the nanocrystals also grows. Below T_g of approximately 994 K, nanoparticle growth primarily occurs through individual crystal growth. Above T_g, the crystal size increases at a faster rate [45,46]. This accelerated growth is attributed to the enhanced diffusivity of the supercooled liquid as the temperature rises. SAED and EDS results confirm that the precipitated nanoparticles are α-Fe (see Fig. S2).

The crystallization behavior of lunar glasses at a depth of approximately 4 μm was investigated *in situ* using TEM during heating. In the absence of irradiated clusters, no structural changes were observed during heating up to 873 K (Fig. 4a, b). HRTEM images and SAED patterns confirmed that the samples retained an amorphous structure at this temperature. At 953 K, nanocrystals with distinct lattice fringes began to appear (inset at the top right of Fig. 4c). However, due to the small size of the nanocrystalline phase, no noticeable contrast changes were observed in the SAED pattern (inset at the lower right of Fig. 4c). These results indicate the early stages of nanocrystallization at this depth.

It is noteworthy that the first distinct nanocrystal in the irradiation layer is observed at 933 K, which is lower than the temperature required for nanocrystallization in the interior

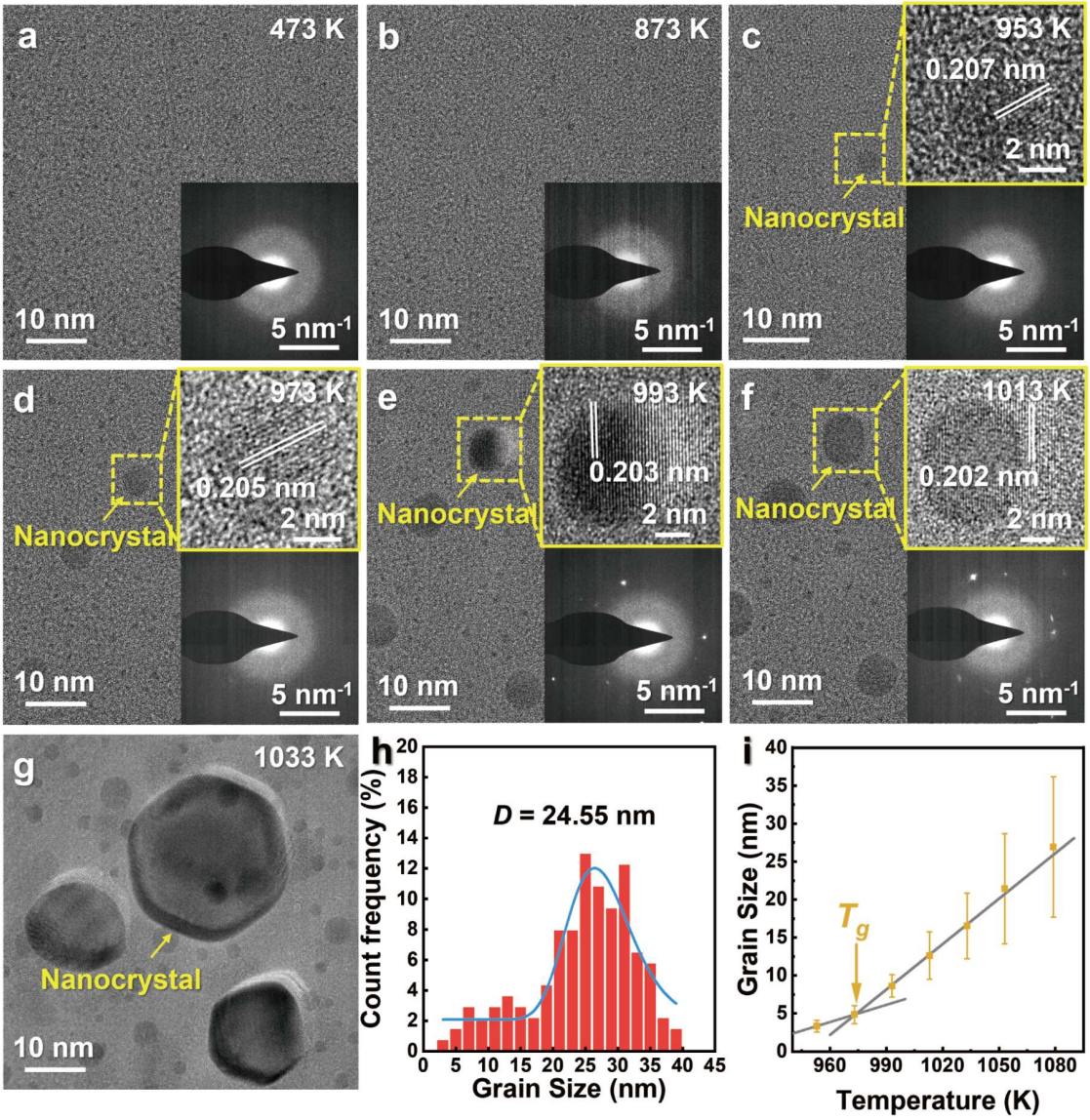

Figure 4 *In situ* HRTEM images and grain size distribution of the interior part in the lunar glass at different stages of *in situ* heating TEM observation. The temperature and holding time at which the images were acquired are (a) 473 K, 10 min; (b) 873 K, 10 min; (c) 953 K, 10 min, the inset shows the lattice fringe is observed; (d) 973 K, 10 min; (e) 993 K, 10 min; (f) 1013 K, 10 min; The insets show the zoomed-in HRTEM images of nanocrystals and corresponding SAED patterns. (g) 1033 K, 10 min. The yellow arrows represent the nanocrystals. (h) The grain size distribution for the irradiation layer in the lunar glass after *in situ* TEM heating. (i) The trend of grain size variation with temperature in the interior part. The intersection of the two grain growth stages represents T_g temperatures of the interior part.

region. At 973 K, abundant nanocrystals are formed (Fig. 4d). When the temperature reaches 993 K, the nanocrystals show significant growth (Fig. 4e). The corresponding SAED pattern (inset of Fig. 4e) displays sharp spots, confirming the progression of nanocrystallization. As the temperature increases from 1013 to 1033 K, the growth rate of the nanocrystals accelerates, which is attributed to the enhanced diffusivity of the supercooled liquid at higher temperatures (Fig. 4f, g). Statistical analysis shows that the average grain size of nanocrystals in the interior region is 24.55 nm, with sizes ranging from 5 to 40 nm (Fig. 4h, i). The broad size distribution reflects the stochastic nature of nucleation and growth processes for Fe nanocrystals.

Nanocrystals larger than 20 nm are typically formed through the merging of smaller nanocrystals. Fig. 5 shows this process, where large nanocrystals are created as smaller ones come into contact and reorient to form a single, larger crystal. The high atomic diffusivity in the supercooled liquid plays a critical role in facilitating this merging process. Therefore, at high temperatures, crystal growth primarily occurs through the absorption or merging of smaller nanocrystals.

The long-term solar wind irradiation will implant abundant H into lunar particles, including lunar glasses. The H stored in lunar glass is beneficial to the formation of these Fe clusters. At high temperatures, H will release and react with lunar glass, forming Fe nanocrystals [31]. Comparing the nanocrystallization behavior of the irradiation layer with that of the interior region, solar wind irradiation significantly lowers the crystallization onset temperature. This leads to a denser precipitation of nanocrystals, which are uniformly distributed within the amorphous matrix. These changes in nanocrystallization behavior provide valuable insights for designing nanocrystalline/amorphous alloys. Controlled nanocrystallization in Fe-based amorphous alloys can enhance their soft magnetic properties compared to their amorphous precursors [47,48]. Achieving a fine and uniform distribution of Fe nanocrystals remains a key objective in the development of advanced soft magnetic materials.

To simulate the effects of solar wind irradiation, hydrogen ion irradiation was applied to $Fe_{86}B_{14}$ (FeB) metallic glass. $Fe_{86}B_{14}$ was selected as the model material due to its properties as an advanced precursor for nanocrystalline materials. Fig. 6 illustrates the impact of hydrogen ion irradiation on the crystallization behavior of Fe-based metallic glass. The original FeB sample exhibits a typical amorphous structure with no detectable short-range clusters (Fig. 6a). After crystallization, the nanocrystals in the original FeB sample are relatively large (Fig. 6b, e). Larger nanocrystal sizes can degrade the soft magnetic properties of the material. In contrast, the structure of the hydrogen ion-irradiated FeB sample shows notable differences after heating. Hydrogen ion irradiation creates an ~10 nm irradiation layer close to the surface of the FeB sample (Fig. 6c). This layer retains an amorphous structure but exhibits a stronger structural fluctuation compared to the unirradiated region (see Fig. S3). Additionally, numerous clusters with distinct contrast differences appear in the irradiation layer, resembling the structure observed in the irradiation layer of lunar glasses. After crystallization, the nanocrystal size in the irradiated layer is significantly smaller than in the unirradiated region (Fig. 6d, f). These results demonstrate that the effect of hydrogen ion irradiation on the crystallization behavior of FeB metallic glass closely mirrors the influence of solar wind on the crystallization behavior of lunar glasses. As Fig. 6g shows, after crystallization, the relative permeability of irradiated FeB is 1442 at 10 kHz, which is 10.2% higher than the unirradiated FeB (1308 at 10 kHz).

The results suggest that hydrogen ion irradiation of Fe-based

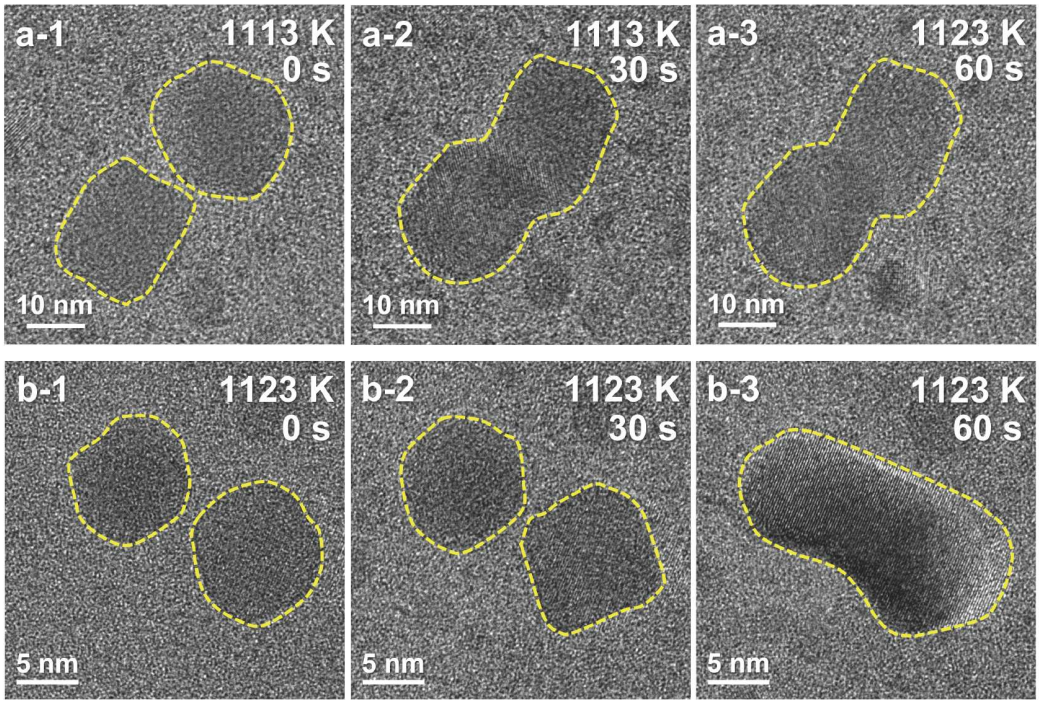

Figure 5 HRTEM images capturing the merging progress of nanocrystals. The temperature and the holding time at which the images were acquired are estimated to be: (a-1) 1113 K and 0 s; (a-2) 1113 K and 30 s; (a-3) 1113 K and 60 s; (b-1) 1123 K and 0 s; (b-2) 1123 K and 30 s; (b-3) 1123 K and 60 s.

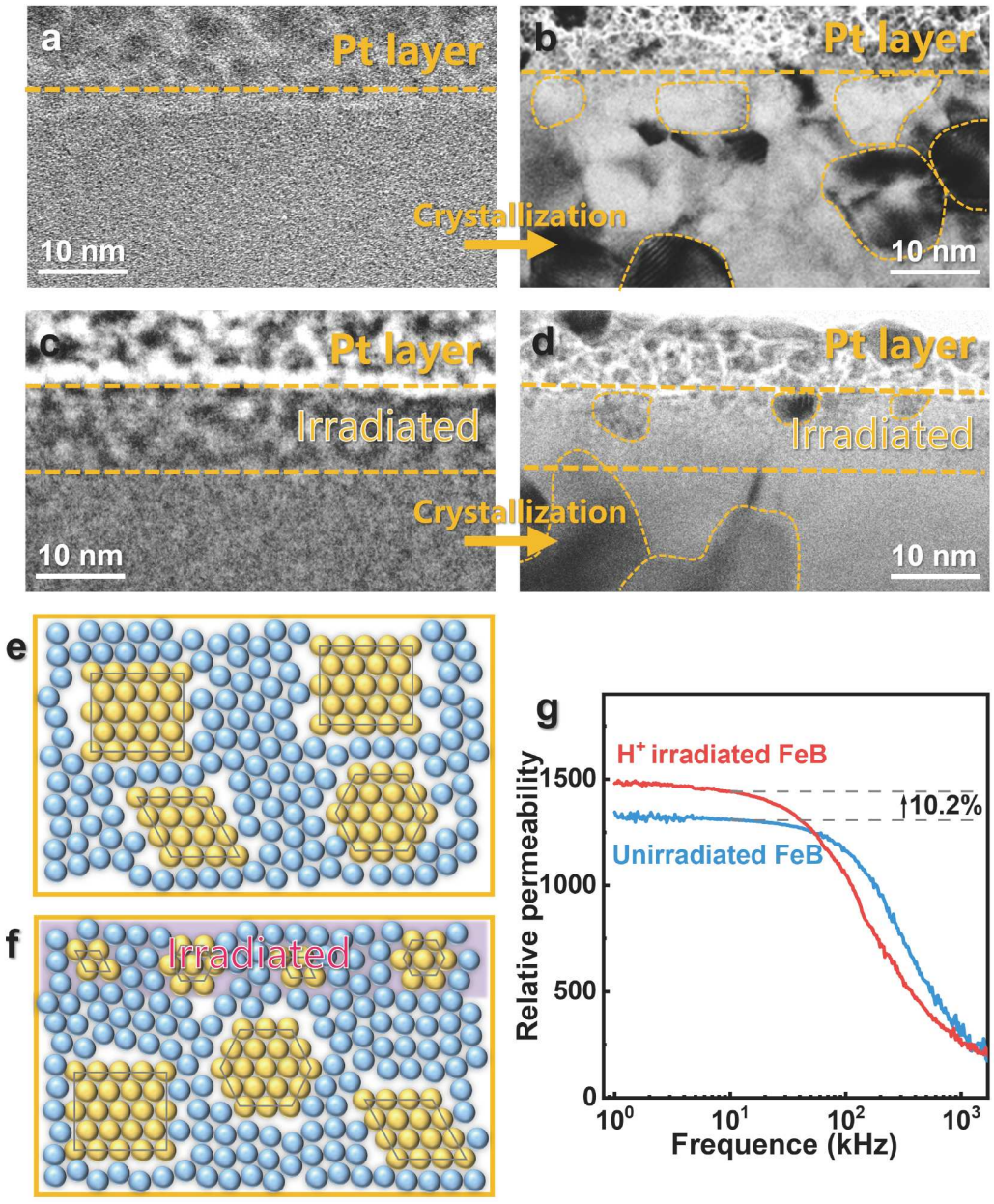

Figure 6 Schematic illustration and HRTEM images of the effect of ion irradiation on the crystallization behavior of FeB metallic glass. (a) HRTEM image of unirradiated glass; (b) HRTEM image of unirradiated glass after crystallization; (c) Defocused HRTEM image of irradiated glass; (d) HRTEM image of irradiated glass after crystallization; (e) Schematic diagram of unirradiated glass after crystallization; (f) Schematic diagram of irradiated glass after crystallization, which is composed of smaller and more uniform nanocrystals; (g) The changes of relative permeability as a function of frequency at 1 A m^{-1} from 1 kHz to 1 MHz for unirradiated FeB after crystallization and irradiated FeB after crystallization, respectively.

metallic glass is an effective method for regulating its crystallization behavior, facilitating the formation of a fine and uniform distribution of nanocrystals. Notably, hydrogen ion irradiation also lowers the crystallization onset temperature of the irradiation layer, which can broaden the temperature window for annealing nanocrystalline soft magnetic materials [49]. This, in turn, promotes the achievement of a more uniform distribution of nanocrystals.

However, the effect of hydrogen ion irradiation is limited to the surface layer, typically extending only a few tens of nanometers deep. Thus, a key challenge for future work is to extend the irradiation effect throughout the bulk material. Despite this limitation, the findings offer a promising approach for improving the soft magnetic properties of Fe-based metallic glasses by controlling their nanocrystallization behavior.

CONCLUSIONS

In conclusion, solar wind and ion irradiation significantly influence the structure and crystallization behavior of glassy materials. For lunar glasses, the irradiation layer formed by solar wind results in the formation of finer nanocrystals with a more uniform distribution upon heating. A similar effect is observed in $Fe_{86}B_{14}$ nanocrystalline soft magnetic materials subjected to hydrogen ion irradiation. This demonstrates that hydrogen ion

irradiation is an effective approach for refining nanocrystals. These findings not only enhance our understanding of the structure and properties of lunar regolith glasses but also provide valuable insights for the design and development of advanced nanocrystalline soft magnetic materials.

Received 20 February 2025; accepted 4 April 2025; published online 27 May 2025

1 Papike JJ, Ryder G, Shearer CK. Planetary Materials. Papike J (ed). Berlin: De Gruyter, 1998, 719–952
2 Taylor GJ, Martel LMV, Lucey PG, *et al.* Modal analyses of lunar soils by quantitative X-ray diffraction analysis. Geochim Cosmochim Acta, 2019, 266: 17–28
3 Delano JW. Pristine lunar glasses: criteria, data, and implications. J Geophys Res, 1986, 91: 201–213
4 Zeigler RA, Korotev RL, Jolliff BL, *et al.* The geochemistry and provenance of Apollo 16 mafic glasses. Geochim Cosmochim Acta, 2006, 70: 6050–6067
5 Zellner NEB. Lunar impact glasses: probing the Moon's surface and constraining its impact history. JGR Planets, 2019, 124: 2686–2702
6 Delano JW, Livi K. Lunar volcanic glasses and their constraints on mare petrogenesis. Geochim Cosmochim Acta, 1981, 45: 2137–2149
7 Taylor SR, Jakeš P. Proceedings of the Fifth Lunar Conference. Houston: The Lunar Science Institute, 1974, 1287–1305
8 Saal AE, Hauri EH, Cascio ML, *et al.* Volatile content of lunar volcanic glasses and the presence of water in the Moon's interior. Nature, 2008, 454: 192–195
9 Saal AE, Hauri EH. Large sulfur isotope fractionation in lunar volcanic glasses reveals the magmatic differentiation and degassing of the Moon. Sci Adv, 2021, 7: eabe4641
10 Shearer CK, Papike JJ. Basaltic magmatism on the Moon: a perspective from volcanic picritic glass beads. Geochim Cosmochim Acta, 1993, 57: 4785–4812
11 Chao ECT, Boreman JA, Minkin JA, *et al.* Lunar glasses of impact origin: physical and chemical characteristics and geologic implications. J Geophys Res, 1970, 75: 7445–7479
12 Delano JW, Zellner NEB, Barra F, *et al.* An integrated approach to understanding Apollo 16 impact glasses: chemistry, isotopes, and shape. Meteorit Planet Scien, 2007, 42: 993–1004
13 Korotev RL, Zeigler RA, Floss C. On the origin of impact glass in the Apollo 16 regolith. Geochim Cosmochim Acta, 2010, 74: 7362–7388
14 Jaret SJ, Woerner WR, Phillips BL, *et al.* Maskelynite formation via solid-state transformation: Evidence of infrared and X-ray anisotropy. JGR Planets, 2015, 120: 570–587
15 Kim HN, Park C, Park SY, *et al.* Partial melting-induced chemical evolution in shocked crystalline and amorphous plagioclase from the lunar meteorite mount DeWitt 12007. JGR Planets, 2019, 124: 1852–1863
16 Noble SK, Keller LP, Pieters CM. Evidence of space weathering in regolith breccias I: lunar regolith breccias. Meteorit Planet Scien, 2005, 40: 397–408
17 Zhao R, Shen L, Xiao D, *et al.* Diverse glasses revealed from Chang'E-5 lunar regolith. Natl Sci Rev, 2023, 10: nwad079
18 Keller LP, McKay DS. The nature and origin of rims on lunar soil grains. Geochim Cosmochim Acta, 1997, 61: 2331–2341
19 Zhang SL, Keller LP. Space weathering effects in lunar soils: the roles of surface exposure time and bulk chemical composition. In: 42nd Lunar and Planetary Science Conference. Woodlands: Lunar and Planetary Inst. 2011, 1947
20 Bibring JP, Duraud JP, Durrieu L, *et al.* Ultrathin amorphous coatings on lunar dust grains. Science, 1972, 175: 753–755
21 Bibring JP, Langevin Y, Maurette M, *et al.* Ion implantation effects in "cosmic" dust grains. Earth Planet Sci Lett, 1974, 22: 205–214
22 Noguchi T, Nakamura T, Kimura M, *et al.* Incipient space weathering observed on the surface of itokawa dust particles. Science, 2011, 333: 1121–1125
23 Heiken GH, Vaniman DT, French BM. Lunar Sourcebook: A User's Guide to the Moon. Cambridge: Cambridge University Press, 1991
24 Chen Z, Zhao Y, Chi X, *et al.* Geological timescales' aging effects of lunar glasses. Sci Adv, 2023, 9: eadi6086
25 Xiao Z, Yan P, Wu B, *et al.* Translucent glass globules on the Moon. Sci Bull, 2022, 67: 355–358
26 Starukhina LV. Polar regions of the Moon as a potential repository of solar-wind-implanted gases. Adv Space Res, 2006, 37: 50–58
27 Li A, Chen X, Song L, *et al.* Taking advantage of glass: capturing and retaining the helium gas on the Moon. Mater Futures, 2022, 1: 035101
28 Liu Y, Guan Y, Zhang Y, *et al.* Direct measurement of hydroxyl in the lunar regolith and the origin of lunar surface water. Nat Geosci, 2012, 5: 779–782
29 Pieters CM, Goswami JN, Clark RN, *et al.* Character and spatial distribution of OH/H_2O on the surface of the Moon seen by M^3 on Chandrayaan-1. Science, 2009, 326: 568–572
30 Zeng X, Tang H, Li XY, *et al.* Experimental investigation of OH/H_2O in H^+-irradiated plagioclase: implications for the thermal stability of water on the lunar surface. Earth Planet Sci Lett, 2021, 560: 116806
31 Chen X, Yang S, Chen G, *et al.* Massive water production from lunar ilmenite through reaction with endogenous hydrogen. Innovation, 2024, 5: 100690
32 Zhou C, Tang H, Li X, *et al.* Chang'E-5 samples reveal high water content in lunar minerals. Nat Commun, 2022, 13: 5336
33 Xu Y, Tian HC, Zhang C, *et al.* High abundance of solar wind-derived water in lunar soils from the middle latitude. Proc Natl Acad Sci USA, 2022, 119: e2214395119
34 He H, Ji J, Zhang Y, *et al.* A solar wind-derived water reservoir on the Moon hosted by impact glass beads. Nat Geosci, 2023, 16: 294–300
35 Shearer CK, Papike JJ, Galbreath KC, *et al.* A SIMS study of lunar "komatiitic glasses": trace element characteristics and possible origin. Geochim Cosmochim Acta, 1990, 54: 1851–1857
36 Li C, Hu H, Yang MF, *et al.* Characteristics of the lunar samples returned by the Chang'E-5 mission. Natl Sci Rev, 2022, 9: nwab188
37 Yan P, Xiao Z, Wu Y, *et al.* Intricate Regolith Reworking Processes Revealed by Microstructures on Lunar Impact Glasses. JGR Planets, 2022, 127: e2022JE007260
38 Yan P, Xiao Z, Wu Y, *et al.* Submicroscopic iron-rich grains throughout impact glasses in Chang'E-5 regolith. Icarus, 2024, 410: 115920
39 Yan P, Xiao Z, Wu Y, *et al.* Adhesion of silicate impact melts on impact glasses of Chang'E-5 regolith. JGR Planets, 2024, 129: e2024JE008777
40 Bradley JP, Ishii HA, Gillis-Davis JJ, *et al.* Detection of solar wind-produced water in irradiated rims on silicate minerals. Proc Natl Acad Sci USA, 2014, 111: 1732–1735
41 Tian HC, Wang H, Chen Y, *et al.* Non-KREEP origin for Chang'E-5 basalts in the Procellarum KREEP Terrane. Nature, 2021, 600: 59–63
42 Hu S, He H, Ji J, *et al.* A dry lunar mantle reservoir for young mare basalts of Chang'E-5. Nature, 2021, 600: 49–53
43 Li QL, Zhou Q, Liu Y, *et al.* Two-billion-year-old volcanism on the Moon from Chang'E-5 basalts. Nature, 2021, 600: 54–58
44 Loeffler MJ, Dukes CA, Baragiola RA. Irradiation of olivine by 4 keV He^+: simulation of space weathering by the solar wind. J Geophys Res, 2009, 114: 2008JE003249
45 Busch R, Johnson WL. The kinetic glass transition of the $Zr_{46.75}Ti_{8.25}Cu_{7.5}Ni_{10}Be_{27.5}$ bulk metallic glass former-supercooled liquids on a long time scale. Appl Phys Lett, 1998, 72: 2695–2697
46 Löffler JF, Schroers J, Johnson WL. Time-temperature-transformation diagram and microstructures of bulk glass forming $Pd_{40}Cu_{30}Ni_{10}P_{20}$. Appl Phys Lett, 2000, 77: 681–683
47 Zang B, Song L, Parsons R, *et al.* Influence of thermal history on the crystallization behavior of high-Bs Fe-based amorphous alloys. Sci China-Phys Mech Astron, 2023, 66: 256111
48 Shen F, Zang B, Song L, *et al.* Ultra-fine microstructure and exceptional low coercivity developed in a high-Bs Fe-Si-B-P alloy by co-alloying Ni, Mo, and Cu. Scripta Mater, 2023, 236: 115666
49 Parsons R, Zang B, Onodera K, *et al.* Nano-crystallisation and magnetic softening in Fe–B binary alloys induced by ultra-rapid heating. J Phys D-Appl Phys, 2018, 51: 415001

Acknowledgement This work was supported by the National Key R&D Program of China (2024YFB3813700), the National Natural Science Foundation of China (NSFC, 52231006, U24A201046, 52222105 and 51922102), the Youth Innovation Promotion Association CAS (2019296), the Zhejiang Provincial Natural Science Foundation of China (LZ22A030001 and LR22E010004), and the Ningbo 2025 Science and Technology Innovation Project (20212ZDYF020030).

Author contributions Chen X performed the experiments with the assistance of Ma B, Li A, Wang J and Yin H. Huang Y and Sun J performed the irradiation treatment. Song L and Wang J performed the DSC experiments. Huang Y and Sun J performed the irradiation experiments. Chen X, Song L, Zhang Y, Gao M, Huo J and Wang J-Q performed the data analysis. Chen X and Wang J-Q wrote the paper with input from all authors. Song L, Zhang Y, Huo J and Wang J-Q supervised the work. All authors discussed the results.

Conflict of interest The authors declare that they have no conflict of interest.

Supplementary information Supplementary materials are available in the online version of the paper.

Xiao Chen received his BS degree in polymer science and engineering from Wuhan University of Technology in 2019. He is currently a PhD candidate in materials physics and chemistry under the supervision of Prof. Jun-Qiang Wang at Ningbo Institute of Materials Technology and Engineering, Chinese Academy of Sciences. His PhD research focuses on the physical properties of and *in situ* resource utilization of glassy materials in lunar regolith.

Lijian Song received his PhD degree in materials physics and chemistry in 2018 under the supervision of Prof. Jun-Qiang Wang at Ningbo Institute of Materials Technology and Engineering, Chinese Academy of Sciences. He is currently a professor at Ningbo Institute of Materials Technology and Engineering, Chinese Academy of Sciences. His research focuses on the relaxation kinetics and crystallization behaviors of metallic glasses.

Yan Zhang received his PhD degree from Tohoku University (Japan) in 2012. Then he worked as a postdoctoral fellow and assistant professor at Tohoku University (Japan) from 2012 to 2020. Now he is a professor at Ningbo Institute of Materials Technology and Engineering, Chinese Academy of Sciences. His research focuses on the preparation and development of amorphous and nanocrystalline soft magnetic materials.

Yongjiang Huang received his PhD degree from Harbin Institute of Technology in 2008. Now he is a professor at Harbin Institute of Technology. His interests mainly focus on bulk metallic glasses and their composites, high-entropy alloys, and additive manufacturing of advanced metallic materials.

Juntao Huo received his PhD degree from the Institute of Physics, Chinese Academy of Sciences in 2012. Now he is a professor at Ningbo Institute of Materials Technology and Engineering, Chinese Academy of Sciences. His research focuses on magnetocaloric and electrochemical functional properties of amorphous alloys.

Jun-Qiang Wang received his PhD degree from the Institute of Physics, Chinese Academy of Sciences in 2010. Then he worked as a postdoctoral fellow at Tohoku University (Japan) and the University of Wisconsin-Madison (USA) from 2010 to 2014. Now he is a professor at Ningbo Institute of Materials Technology and Engineering, Chinese Academy of Sciences. His research interests include non-equilibrium thermodynamics and functional properties of glassy materials.

从月壤玻璃到先进金属玻璃材料: 离子辐照诱导致密纳米晶化

陈霄[1,2], 马本舜[1,2], 宋丽建[1*], 张岩[1,2*], 黄永江[3*], 孙剑飞[3], 许巍[1], 李傲[1], 王家宁[1,2], 尹航博策[1], 臧博闻[1], 高萌[1], 赵少凡[4], 姚伟[4], 邹志刚[4,5], 杨孟飞[4], 汪卫华[2,4,6,7], 白海洋[2,4,6], 霍军涛[1,2*], 王军强[1,2*]

摘要 纳米晶化是制备高性能玻璃材料的重要方法. 本研究深入研究了嫦娥五号月壤玻璃微结构及高温晶化行为. 发现月壤玻璃表面4 μm深度范围内存在大量尺寸约2 nm的纳米级缺陷, 分析表明这些缺陷是由太阳风H辐照还原产生的Fe团簇. 热处理过程中, 这些缺陷作为形核位点, 促使析出均匀致密的Fe纳米晶. 相较而言, 月壤玻璃内部未受辐照的区域Fe纳米晶形核具有更强的随机性, 其位置和尺寸波动较大. 受此启发, 通过H^+离子辐照$Fe_{86}B_{14}$金属玻璃体系, 纳米晶化退火后, 在近表面区域获得5–8 nm的纳米晶, 显著小于未辐照样品的晶粒尺寸(15–20 nm), 使磁导率提升10.2%. 以上结果不仅揭示了月壤玻璃的热稳定性, 也提出了一种通过辐照调控纳米晶尺寸优化金属玻璃软磁性能的新方法.